Internal Damage Evolution in Double-Network Hydrogels Studied by Microelectrode Technique

Honglei Guo[1,2], Wei Hong[3,2,4], Takayuki Kurokawa[1,2], Takahiro Matsuda[5], Zi Liang Wu[1,6], Tasuku Nakajima[1,2,7], Masakazu Takahata[8], Taolin Sun[1,2,9], Ping Rao[5], Jian Ping Gong[1,2,7]*

[1]Faculty of Advanced Life Science, Hokkaido University, Sapporo, 001-0021, Japan

[2]Soft Matter GI-CoRE, Hokkaido University, Sapporo, Japan

[3]Department of Mechanics and Aerospace Engineering, Southern University of Science and Technology, Shenzhen, 518055, China

[4]Department of Aerospace Engineering, Iowa State University, Ames, Iowa 50011, United States

[5]Graduate School of Life Science, Hokkaido University, Sapporo, 001-0021, Japan

[6]Ministry of Education Key Laboratory of Macromolecular Synthesis and Functionalization, Department of Polymer Science and Engineering, Zhejiang University, Hangzhou 310027, China

[7]Institute for Chemical Reaction Design and Discovery (WPI-ICReDD), Hokkaido University, N21W10, Kita-ku, Sapporo, Hokkaido, 001-0021, Japan

[8]Faculty of Science, Hokkaido University, Sapporo, 060-0810, Japan

[9]South China Advanced Institute for Soft Matter Science and Technology, South China University of Technology, Guangzhou 510640, China

*Corresponding author

Telephone/Fax: +81-11-706-9011, E-mail: gong@sci.hokudai.ac.jp

Abstract

Double-network (DN) hydrogels have attracted considerable attention owing to their unique mechanism to show extraordinary mechanical strength and toughness. Although the toughening mechanism of the DN gels, breaking of the relatively stiff and brittle first network as sacrificial bonds, is widely accepted, the microstructure and morphology evolution of the internal damage has hardly been revealed. In this study, we study the internal structures of the first network in partially damaged DN gels by using the microelectrode technique (MET), based on the Donnan effect of the polyelectrolyte first network. We measure the spatial distribution of the electric potential of the pre-stretched and then re-swelled DN gels. From the anisotropic depth profiles of potential and re-swelling ratio, the microstructures of DN gels at a scale larger than the microelectrode probe size (~ 200 nm) are revealed at the pre-yielding, yielding, and strain-hardening regimes.

Introduction

Hydrogels are promising biomaterials for artificial organs owing to the high water content and soft properties, similar to natural tissues.[1] To mimic load-bearing bio-tissues such as cartilage, one would have to improve the strength and toughness of hydrogels. Double network (DN) hydrogels, initially developed by Gong's group in 2003, have excellent mechanical properties comparable to those of human cartilage.[2,3] A DN hydrogel consists of two interpenetrated polymer networks with contrasting structural and mechanical characteristics: the first network is stiff but brittle, while the second is compliant and stretchable. Such DN hydrogels were initially developed by using the abundantly cross-linked polyelectrolytes as the first network and the loosely cross-linked neutral polymers as the second network.[2] The polyelectrolyte hydrogel swells extensively in water owing to the counter-ions-induced osmotic pressure, forming a highly stretched, brittle network and leaving ample space for the polymer chains of the second network.

Despite the high water-content (~ 90 wt%), DN gels exhibit unprecedented mechanical properties. For example, the DN gels consisting of poly(2-acrylamido-2-methylpropanesulfonic acid) (PAMPS) as the first network and polyacrylamide (PAAm) as the second network are relatively stiff (elastic modulus of 0.1-1.0 MPa), very strong (tensile strength of 1-10 MPa), stretchable (tensile failure strain of 1000-2000 %), and extremely tough (tearing fracture energy of 10^2-10^3 J/m^2).[4]

It has been shown that such a strengthening/toughening effect is universal, independent of the specific polymer chemistry. For example, tough DN gels from

61 diverse pre-stretched neutral polymer networks as the first network have been
62 developed using the molecular stent method.[5] Additionally, tough double-network and
63 triple-network elastomers have also been developed.[6,7]

64 Previous studies[4,8,9] have related the extraordinary toughness of DN gels to the
65 distributed damage of the first network, which dissipates a large amount of energy. Thus,
66 the covalent bonds of the first network serve as sacrificial bonds, providing toughness
67 for the DN gels. Tough DN gels exhibit large hysteresis on the stress–strain curves and
68 a strain–softening behavior similar to the Mullins effect[10,11] of rubbers owing to the
69 extensive internal fracture of the brittle first network.[8,9]

70 For the DN gels, the typical tensile behavior of the samples shows three regimes
71 during loading: the pre-necking regime, in which the stress increases with the strain;
72 the necking regime, in which the stress plateaus at a constant value, independent of the
73 strain, and a narrow necking zone appears and gradually devours the entire sample with
74 the increase of strain; and the hardening regime, in which the stress increases with the
75 strain again.[8] Upon unloading, a sample may swell further in water because of the
76 partial damage in the brittle first network locally releases the constrained second
77 network, and a new osmotic balance may be reached by absorbing more water. Based
78 on the mechanical hysteresis and re-swelling behavior of PAMPS/PAAm DN gels, an
79 internal damage mechanism was proposed.[12] In the pre-necking regime, the load was
80 mainly carried by the first network. Although some short strands of the first network
81 break, the damaged regions are far from percolating. In the necking regime, the cracks
82 percolate, fragmenting the first network into discontinuous islands. As the region

between the fragments are only connected by the soft and stretchable second network, the material softens significantly, leading to the necking phenomenon. In the hardening regime, the fragments of the first network further break into smaller islands due to strain hardening of the second network at large stretching.

Some structural analyses have been performed to examine the microstructures of partially damaged DN gels. When the heterogeneous model of DN gel was firstly proposed, the presence of "voids" in the first network PAMPS was deduced according to the result of dynamic light scattering (DLS)[13], varying the molecular weight of the polymer PAAm[14], and mechanical experiment[15,16]. Using small-angle neutron scattering (SANS) technique, it was revealed that the heterogeneity in a PAMPS/PAAm DN gel, after a small compression (~ 50% strain), had a characteristic length of about 1.5 μm.[17] According to the result of wrinkled morphology of ultra-thin DN gel[18] and anisotropic re-swelling behavior,[12] those fragments were considered as rectangular or plate-like structure. Assuming that the dissipated energy is used for the fragments formation through breakage of the covalent bonds, a characteristic size of about 100 nm has been estimated, at a tensile strain of 1,100%, for typical DN gels.[4] However, there are few direct evidences to verify the assumed microstructure changes during the tensile deformation. How the size changes with respect to the tensile strain, corresponding to the heterogeneous fragmentation of PAMPS networks, is yet unclear. A method to directly probe the microstructures of partially damaged DN gels is required.

A polyelectrolyte gel has macro-ions fixed on the polymer network and small counter-ions localized inside the network frame. This concentration difference of the

105 counter-ions between inside and outside of the hydrogel leads to an electric potential
106 difference, known as the Donnan potential, between the polyelectrolyte gel and the bath
107 solution. Therefore, by measuring the spatial distribution of the electric potential in a
108 polyelectrolyte hydrogel, one can determine the local counter-ion density, which
109 directly reveals the local structure of the hydrogel. The microelectrode technique (MET)
110 is widely used for detecting the electric potentials in living cells, in neurons reacting to
111 stimuli, and in live animals.[19] Recently, some co-authors succeeded in applying the
112 MET for detecting the electric potential of brittle polyelectrolyte hydrogels by using an
113 extremely thin capillary electrode.[20] This technique allows the accurate probing of the
114 spatial distribution of polyelectrolyte density from the depth profile of the electric
115 potential inside the hydrogels with a spatial resolution in the order of probe size.

116 In this study, we study the microstructural evolution of partially damaged DN
117 hydrogels by measure the electric potential distribution of the re-swelled samples. As
118 shown by previous works, the internal fracture of the polyelectrolyte first network
119 results in anisotropic re-swelling of the DN gels,[12] which indicates a decreased
120 concentration of the first network in the fractured region and enhanced structure
121 heterogeneity. By measuring the evolution of the electric potential distribution with the
122 pre-stretched strains that have been experienced by the samples, we can elucidate the
123 structure change of the first network induced by internal fracture. Firstly, the DN gels
124 are uniaxially stretched to various strains, and then the samples are re-swelled in water.
125 The anisotropic re-swelling behavior of damaged DN hydrogels in different stretch
126 regimes is characterized. Then, the depth profiles of the electric potential of the pre-

stretched DN gels in the re-swollen state are measured using the MET from the three directions of the samples. From the potential variation, the anisotropic microstructure of the fractured PAMPS network is elucidated. Furthermore, the structure at the boundary of the necked and un-necked zones is also studied using the MET to reveal the origin of the necking phenomenon.

EXPERIMENTAL

Materials

2-Acrylamido-2-methylpropanesulfonic acid (AMPS) was provided as a courtesy from Toa Gosei Co., Ltd and used as received. Acrylamide (AAm) purchased from Junsei Chemical Co., Ltd was recrystallized from chloroform. *N,N′*-methylenebisacrylamide (MBAA), 2-oxoglutaric acid (OA), and potassium chloride (KCl) were purchased from Wako Pure Chemical Industries, Ltd and used as received.

Synthesis of DN hydrogels

DN hydrogels were synthesized according to the previous report[2]. Briefly, the first network of PAMPS gels, coded as 1-4-0.6, was prepared via radical polymerization, from an aqueous solution containing 1 M AMPS monomer, 40 mM MBAA as a cross-linker, and 6 mM OA as an initiator. The precursor solution was poured into a reaction cell consisting of two glass plates spaced with 1 mm silicone rubber. PAMPS hydrogels were obtained after ultraviolet (UV) irradiation for 8 h in an argon atmosphere. Then, the PAMPS gels were immersed into an aqueous solution containing 2 M AAm monomer and 0.2 mM OA for 1 d. The swollen gels were sandwiched between two

glass plates and UV irradiated for 8 h in an argon atmosphere for the second polymerization of PAAm. Subsequently, DN gels were obtained and immersed into pure water for about one week until equilibrium was reached. No chemical cross-linker was added in the polymerization of the second network and the PAAm chains were chemically connected to the PAMPS network via the residual cross-linkers of the PAMPS network.[21]

Mechanical tensile tests

A tensile test was performed using a universal mechanical test machine (Tensilon RTC-1150A, Orientec Co.). The swollen DN gels, of 2.51 mm-thick, were cut into dumbbell-shaped specimens with standardized JIS K 6251-7 sizes (length of 35 mm, width of 2 mm, and gauge length of 12 mm) with a gel cutting machine (DumbBell Co., Ltd.). The DN specimens were stretched to different strains at a constant velocity of 100 mm/min at room temperature. In this work, the stress σ refers to the nominal stress, defined as the tensile force divided by the cross-section area of the un-deformed sample, and the engineering strain, ε, is defined as the change in the gauge length divided by the gauge length of the un-deformed sample.

Re-swelling ratio measurements

To measure the re-swelling ratios at different positions, the dumbbell-shaped DN gel with a gauge length of 12 mm was divided into 11 sections by markers (0.1mm in width, 1 mm in distance) using a plastic mask before stretching (**Figure 2a**). The spaced

markers were printed onto the gel surface by using hydrophobic white ink with the aid of a mask that is made by a computer-controlled laser cutter. Then the DN gel was stretched uniaxially to a prescribed strain and then unloaded. The stretched sample was re-swelled in pure water for 2 d until equilibrium was reached. After that, the width, thickness, and length of each different section was measured according to the markers. The linear re-swelling ratios between the re-swollen state and the virgin state prior to stretching, denoted as λ_w, λ_t, and λ_l for the width, thickness, and length directions, were calculated. The volume re-swelling ratio, q, was estimated as $q= \lambda_w\lambda_t\lambda_l$. For the necking samples with coexisting necked and un-necked zones, λ and q values were obtained from sections of the two types of regions. After that the size measurement, the re-swollen samples were transferred into the reference KCl solution for more than 2 d until equilibrium was reached.

Potential measurement

The electrical potential ϕ of the samples in relative to the bath solution was measured by using the MET, according to our recent report.[20] Briefly, the microelectrodes were prepared by placing a reversible silver/silver chloride electrode into a glass capillary. Depending on the experiments, the tip diameter of the capillary was varied between 100 and 1500 nm. The glass capillaries were prepared by pulling a borosilicate glass tube (outer diameter of 1.00 mm, inner diameter of 0.78 mm) using a horizontal automatic micropipette puller (P-2000, Sutter) and then filled with a 3 M KCl solution and connected to the inputs of a high-impedance intracellular preamplifier

193 (Model 8700 Cell Explorer, Dagan). A carbon electrode, which was placed in the bath
194 solution, was used as the reference electrode. The re-swelled DN gels, which had
195 thickness of 2.5–5.0 mm depending on the pre-stretch ratio, was immersed in a 10^{-5} M
196 KCl solution for equilibrium prior to the measurement. A glass microelectrode
197 controlled using a micromanipulator (DMA-1511, Narishige) was inserted into the
198 hydrogel at a constant speed of 0.4 μm/s. The output signals were recorded using an
199 oscilloscope (Iwatsu, DS-4264) in the real-time mode. The electrical potential signals
200 were collected at 100 sampling per second. All the measurements were performed at
201 25 °C. The spatial resolution from the micromanipulator in the depth profile of the
202 insertion direction was 5 nm. Unless otherwise specified, the potential measurements
203 were performed by using a microelectrode with tip diameter 170–200 nm, and the
204 obtained potential values were the average over this length scale.

205 It should be noted that the residual chemicals due to the uncompleted reaction in
206 the DN synthesis should be carefully removed before the potential measurement. The
207 leakage of the residual ionic monomers from the DN gels would increase the ionic
208 strength of the reference solution, leading to a decrease in the measured potential value.
209 We have confirmed that to reduce the leakage of the chemical residuals to a level that
210 causes negligible change in the ionic strength of the reference solution (KCl =10^{-5} M),
211 the DN gels should be repeatedly washed in a large amount of deionized water for more
212 than one month. In this paper, unless specifically mentioned, the DN gels were washed
213 in a large amount of deionized water for approximately one week before stretching, and
214 then further washed in deionized water for another one week prior to the MET

measurements. Such samples still contained residual chemicals, resulting in an increase in the ion concentration in the reference solution. From the potential difference (~ 38 mV) measured after one-month washing and after two-weeks washing, the ionic strength of the reference solution was estimated as 4.4×10^{-5} M, which is several times higher than the pre-set reference solution ($C_{KCl} = 10^{-5}$ M) due to leakage of residual chemicals from the short washed DN gels. Accordingly, the potentials measured in this study were relative to the reference solution with an effective ionic strength of 4.4×10^{-5} M, and were approximately ~ 38 mV lower in absolute value than those measured with the pre-set reference solution of 10^{-5} M KCl.

Results and discussion

Re-swelling ratio of pre-stretched DN gel

The stress–strain curve of the DN gels used in this study, as shown in **Figure 1**, well reproduces the typical stress–strain curve of a conventional DN gel, showing the three deformation regimes. The re-swelling behavior of the DN gels after different degrees of pre-stretching is shown in **Figure 2**. During re-swelling, a DN sample increases its size in all directions, but exhibits strong anisotropy. The linear re-swelling ratios in the length direction are much larger than those in the width and thickness directions, as shown in **Figure 2b**. In the necking regime, where the softened zone (the narrow necked part) and unsoftened zone (the thick unnecked part) coexist as shown in **Figure 1**, two different degrees of re-swelling are observed as illustrated in **Figure 2a**. The re-swelling of the softened zone is much larger than the unsoftened zone in all the

three directions, and all the data show a slight increase with the increase of the pre-strain. This is consistent with the slight increase of the stress in the necking regime, indicating that the internal structure of the PAMPS network is further damaged with the increase of the strain, both in the unsoftened and softened zones. In the hardening regime, where the unsoftened zone disappears, and the sample deforms homogeneously (**Figure 1**), the whole sample shows a homogeneous re-swelling. The volume re-swelling ratios q, which is the product of the re-swelling ratio of the three directions, is shown in **Figure 2c**. q increases with the pre-stretch level and become significantly large. The result is consistent with the previous results on the anisotropic internal damage of uniaxially stretched DN gels.[12]

Electrical potential distribution of pre-stretched DN gel

Here, we use the MET to examine the microstructure evolution of the DN gels after stretching and unloading. From the equilibrium condition of electrochemistry, the Donnan potential, ϕ, i.e. the electrical potential difference between the gel and the solution, is related to the ratios of mobile-ion concentration C and activity coefficient γ between deep in the gel (g) and the bath solution (s):[22]

$$\phi = \frac{2.3RT}{zF}\log\frac{\gamma_{\mathrm{s}}C_{\mathrm{s}}}{\gamma_{\mathrm{g}}C_{\mathrm{g}}}. \quad (1)$$

Here, z is the valence of the mobile ion in consideration, R is the gas constant, T is the absolute temperature, and F is the Faraday constant. The subscripts g and s denote the parameters in the gel and in the solution, respectively. When the salt concentration in the bath solution is significantly lower than the macro-ion concentration of the

hydrogels, the average concentrations of macro-ions and the mobile counter-ions over a length scale significantly larger than the mesh size of the network (on the order of nanometers) are equal, as required by the charge-neutrality condition. Thus, by using a microelectrode probe with a diameter significantly larger than the mesh size, we can measure the local average concentrations of mobile counter-ions and the macroions with a spatial resolution determined by the microelectrode probe size. Since the PAMPS network in a DN gel has a strong concentration fluctuation at length scales much larger than the mesh size of the network due to inhomogeneous chemical crosslinking,[23] this MET method can probe the spatial charge density variation at a scale larger than the probe size. To select a proper probe size, first, we measured the potential of a virgin DN gel by using microelectrodes of different tip diameters in the range of 100 ~ 1000 nm. This size range is significantly larger than the mesh size of the PAMPS network[23]. As shown in **Figure S1(a)**, the potential measured by microelectrodes with thick tips (d > 200 nm) is independent of the probe size, showing a value well in agreement with the theoretical value estimated from the bulk average concentration of PAMPS, while that measured by thin microelectrodes (d < 200 nm) decreases with the probe size. Furthermore, a thin microelectrode shows a spatial fluctuation of potential (**Figure S1(b)**) while a thick microelectrode does not (**Figure S1(c)**). These results clearly show that thin probe measurements are affected by the spatial variation of charge density while thick electrode measurements reflect the averaged potential in a large-scale. The deviation of the potential measured by thin electrodes towards smaller values indicates that the soft regions with low PAMPS concentration is sampled more often due to less

volume exclusion effect of the thin electrodes. In this study, we use a probe of tip diameter d =170 – 200 nm, large enough to measure the average structure of the virgin DN gels but small enough to probe the microstructure induced by internal damage of the DN hydrogels.

For a pre-stretched and then re-swelled DN gel with a volume re-swelling ratio q relative to its virgin gel, the potential ϕ of the gel relative to the potential of its virgin DN gel, ϕ_0, is theoretically related to q as

$$\phi = \frac{2.3RT}{zF}\log\frac{\gamma_s C_s}{\gamma_g C_g'} = \frac{2.3RT}{zF}\log\frac{\gamma_s C_s}{\gamma_g C_g/q} = \phi_0 + \frac{2.3RT}{zF}\log q\,, \qquad (2)$$

where C_g' is the PAMPS counterions concentration of the re-swollen sample, and C_g is the counterions concentration of the virgin DN gel. In **Eq. (2)**, we assume that the activity coefficient of counterions in the gel, γ_g, does not vary with the re-swelling ratio. The theoretical value of $2.3RT/zF$ for the PAMPS network with positive mono-valent counter-ions (z = +1) at 298 K is 59 mV. **Eq. (2)** has been experimentally confirmed by using MET for PAMPS gels.[20] So we can quantitatively estimate the local swelling ratio of the damaged DN gel from the potential profiles using **Eq. (2)**.

Figure 3a schematically illustrates the shape of re-swelled sample after being pre-stretched to the necking regime. It should be noticed that the sample surfaces perpendicular or parallel to the tensile direction, in the y,z-plane or x,z-plane, respectively, were cut surfaces, and the surface parallel to the tensile direction in the x,y-plane was un-cut surface. **Figure 3b** shows the depth profiles of the electrical potential for the DN gel measured from the x,y-plane of the re-swollen sample subjected to different pre-stretching strains. The electric potential drastically decreased

from zero at the gel-solution interface, and then plateaued at negative values, except for some spatial fluctuations. The virgin DN gel ($\varepsilon = 0$), showed the largest potential drop. The pre-stretched samples showed smaller potential drops, and the values decreases with the increased strains.

The average bulk electrical potentials of re-swollen DN gels pre-stretched at different strains are shown in **Figure 3c**. In the pre-necking regime, the potential values were amplitude decrease than that of virgin DN gel, indicating that a decreased charge density of the PAMPS networks in the DN gel. In the necking regime, where the softened zone and unsoftened zones co-existed, the electrical potential in the unsoftened zone showed only a small decrease in relative to that in the pre-necking regime, while the potential in the softened zone exhibited a very large change towards the amplitude decrease direction. Moreover, the absolute values of the potential in the necking regime slightly decreased with the further increase of the strain, both for the softened and unsoftened zones. This phenomenon is in consistent with the slight increase of the stress in the stress–strain curve (**Figure 3c**, upper figure), the increase of the re-swelling ratio (**Figure 2b**, **c**), and the varied retardation under circular polarized optical observation (supporting information **Figure S2**). These results indicate that even in the necking regime, the PAMPS networks in the co-existed softened and unsoftened zones were further fractured slightly with the increase of the strain. In the hardening regime, the potential values became amplitude decrease, clearly indicating that the PAMPS network is further diluted by internal-fracture-induced re-swelling.

To see the correlations between the pre-stretch-induced potential changes and the

pre-stretch-induced re-swelling ratio changes of the sample, we plot the average potential drop ϕ against the logarithmic volume re-swelling ratio log q in **Figure 3d**. All experimental data points fall on a straight line, approximately,

$$\phi/\mathrm{mV} = -155 + 110 \log q\,. \quad (3)$$

The slope is obtained, from linear regression by using the data on **Figure 3d**, to be 110 mV, which is about two times of the theoretical value of 59 mV from **Eq.2**, and the measured potential drops are lower than the values estimated from the average re-swelling ratio q by using **Eq. (2)**. The larger the re-swelling ratio q, corresponding to a more heterogeneous microstructure, the more the potential deviation. This increase in the potential deviation indicates the enhanced heterogeneous microstructure for samples with increased pre-stretching. This is because a decrease in the electrode size relative to the spatial heterogeneity leads to a decrease in the measured potential due to the same reason of the electrode size dependence as seen for a non-stretched virgin DN gel (**Figure S1**). For samples experienced large pre-stretching strains, the inter-fragment regions of PAMPS network, which is relatively soft with low chain density of the PAMPS network, are more likely to be probed by the electrode, leading to more pronounced deviation from the average values of potential.

Structure anisotropy and heterogeneity induced by internal fracture

To reveal the structure anisotropy induced by tensile deformation, we further measured the potential of the samples from the two cut surfaces (y,z- and x,z-planes) and compared the results with those for the virgin surface (x,y-plane), as shown in

Figure 4. For comparison, the results measured from the x,y-plane are also shown in the figure. Thicker gradient layers of 25–70 μm were observed in the potential curves measured from the cut surfaces on virgin samples (ε=0), and in the unsoftened zone of necking (ε=5.53) samples, compared to those from the non-cut surface. These gradient layers imply the existence of damaged zones caused by cutting. No gradient layer was observed in the softened zone (ε = 5.53 and 8.25) of the necking samples and the hardening sample (ε=15.34), owing to the bulk internal damage of the samples under large pre-stretching.

The average potential values in the bulk of the samples measured from the y,z- and x,z-planes were quite close to those measured from the x,y-plane, as shown in **Figure 4**. These bulk results measured from the y,z- and x,z-planes are also added in **Figures 3c, d** for comparison. However, the fluctuation of the potential profiles, which reveals the concentration fluctuation of the PAMPS network, is distinctly anisotropic for the pre-stretched samples. For clarity, the enlarged potential profiles in the bulk regions measured from the three surfaces for the virgin (ε = 0) and pre-stretched (ε = 8.25, softened zone) samples are shown in **Figures 5a** and **5b**, respectively. No potential anisotropy is observed for the virgin sample, while the pre-stretched samples shows distinct anisotropy in the potentials. A large spatial fluctuation of $\xi = 4.66 \pm 3.26$ μm is clearly observed for the profile from the y,z-plane, along the direction of pre-stretching. On the other hand, the profiles from the x,y-plane and x, z-plane, in parallel to the pre-stretching direction, are much smoother. These results clearly show the anisotropy in the internal fracture of the PAMPS network.

Next, we observe how the potential fluctuation changes with respect to the pre-stretch strain. **Figure 5c** shows the potential profiles in the stretching direction measured from the y,z-plane at different pre-stretched strains. For the virgin sample, the potential fluctuation is small (in the range of -145 to -170 mV). The fluctuation level first increases and then decreases with the pre-stretched strain. The potential fluctuation in the softened zone of necking sample pre-stretched at strain $\varepsilon = 5.53$ ranges from -80 to -120 mV. The average distance between neighboring valleys at this pre-stretched strain is approximately $\xi = 4.46 \pm 2.52$ μm. With further damage in the gel, both the fluctuation and the average distance increase; e.g. the average distance in the softened zone increases to $\xi = 4.66 \pm 3.26$ μm at a pre-stretch strain of $\varepsilon = 8.25$. When the sample is in the strain-hardening regime after the stress plateau in the stress-strain curve, i.e., when the entire sample is softened, the potential fluctuation reduces, while the average distance between potential valleys further increases (e.g., $\xi = 5.66 \pm 4.45$ μm at a pre-stretch strain of $\varepsilon = 15.34$).

If two damaged PAMPS fragments are only connected by the second network PAAm with inter-fragments distance comparable to or larger than the electrode diameter, the minimum potential values of re-swelled DN gels should be very close to that of the second PAAm networks (which is approximately -10 ~ -30 mV, slightly more negative to the potential of the pure PAAm gel due to co-polymerization of the residual AMPS monomer into the second network). In fact, much large negative potentials were measured at softened zone and hardening zone, as shown in **Figure 5b**. This suggests that the fracture occurs at various length scales. To characterize the multi-scale structure

391 change induced by internal fracture of the PAMPS network, we performed a statistical
392 analysis on the potential fluctuation profiles obtained along the pre-stretch direction
393 (y,z-plane) for each pre-stretch strain. The measured potentials are analyzed according
394 to the probability density, as shown by the histograms with a sampling step of 1.5 mV
395 (**Figure 6**), at various pre-stretch strains. The statistical data are taken from the potential
396 profiles of bulk regions in an observation window of ~ 27 μm (**Fig. 5c**). Prior to any
397 deformation or damage, at $\varepsilon = 0$, the potential exhibits a unimodal distribution over a
398 relatively narrow range (-165 to -148 mV) (**Figure 6a**), which indicates a relatively
399 homogeneous structure. Upon damage, the potential distribution widens, and turns into
400 bimodal (**Figures 6b-f**), especially for the softened zone on a necked sample, as shown
401 in **Figures 6c** and **6e**.

402 By fitting the histograms of the measured potential data with unimodal or bimodal
403 Gaussian distributions, we summarize the peak potentials, full width at half maximum
404 (FWHM), integral area fraction of high potential peak (peak 1) in **Table 1**. Obviously,
405 with increasing the pre-stretched strains, the peaks shift to lower potential values, which
406 indicates that the densities of PAMPS networks decrease by internal fracture-induced
407 swelling. FWHM increases with the pre-stretch strains in the necking regime, both in
408 unsoftened zone and in softened zone. The widening of the potential distribution,
409 especially the splitting from the unimodal to the bimodal distribution, reflects the
410 increase in the structural heterogeneity caused by internal damage of the PAMPS
411 networks: the PAMPS networks fractures to form parts with relatively high charge
412 density (the PAMPS fragments) and low charge density (the inter-fragment regions).

With the increase of the pre-stretch strains, the intensity of the high-potential peak decreases while that of the low-potential peak increases, indicating that the high-density parts gradually break, giving way to low-density parts. When the sample is further stretched to the hardening regime, the high-density parts almost disappear, and potential distribution becomes almost unimodal again, and the corresponding FWHM values decrease, as shown in **Figure 6f**. This suggests that the high-density parts of the PAMPS network fracture and the corresponding PAMPS fragments become homogeneous again in the hardening regime. The evolution of the high- and low-density distributions can be characterized quantitatively by a parameter, f_A, defined as the volume fraction of the high-density parts of PAMPS networks, corresponding to the integral area fraction of high potential peak in **Figure 6**. With the fracture of the DN gel, f_A decreased from 1 to 0.80~0.88 in unsoftened zone, and to 0.42 ~ 0.50 in softened zone of yielding regime, and further to 0.26 in hardening regime (**Table 1**).

Morphology evolution of internal damage in DN gel

From the potential distribution transformation from unimodal to bimodal, the PAMPS network fractures, separating the homogeneous DN gel into parts of high charge density and low charge density. The average size of bimodal structure is several μm for re-swelled samples, as seen from the analysis in **Figure 5**. Both potential peaks shift to lower values, indicating that both parts experience further damage. The high-charge-density parts and low-charge-density parts experience minor and major damage, respectively. Both parts will swell further when immersed in water. The parts of minor

damage, with connected PAMPS networks, swell less; while the parts of major damage swell more owing to the pullout of the PAAm chains from the fragmented PAMPS network. As a result, the minor damaged parts show a relatively higher potential than the major damaged parts. From the values of the two peak potentials (**Figure 6**), the average charge concentration in the parts of minor damage in the softened zone, for example, is estimated to be 4.2~5.2 times that in the parts of major damage.

Let q_1 and q_2 be the re-swelling ratios of the parts with minor and major damage, respectively, and q be the average re-swelling ratio of the gel. The volume fraction of the parts with minor damage after re-swelling, α, is related to the same volume fraction prior to re-swelling α_0 by

$$q\alpha = \alpha_0 q_1. \tag{4}$$

Similarly, the re-swelling ratios of different parts are also related as

$$\frac{1}{q} = \frac{\alpha}{q_1} + \frac{1-\alpha}{q_2}. \tag{5}$$

Estimating the volume fraction α from the probability density distribution (**Figure 6**), and the re-swelling ratios q_1 and q_2 from the potential peaks by using **Eq. (2)**, we list the results in **Table 2**, together with those directly measured. The average re-swelling ratio q calculated from **Eq. (5)** agrees reasonably well with that determined from the volume change of the samples.

It can be found that the re-swelling ratios gradually increase with the pre-stretch strain. The volume fractions, α and α_0, of the parts with minor damage after and before re-swelling, respectively, gradually decreases with the increase of the pre-stretch strain. The volume fraction α of the re-swollen state is slightly smaller than that before

re-swelling, α_0, due to the relatively small swelling ratio of the parts with minor damage. In the hardening regime, α_0 decreases to 0.28 at the pre-stretch strain of 15.53, which means that about 72% of the total volume before re-swelling is taken by the parts with major damage.

T

h

e

Necking occurring from surface to bulk

c Finally, we reveal where the necking initiates. As mentioned previously, the pre-

stretched gel sample in the necking regime exhibited two co-existed zones: softened

zone and un-softened zone. Using polarized optical microscopy, we observed a small

transition zone between these two zones, of thickness ~ 1.7 mm in the unloaded state

(**Figure S3**, supporting information). During the tensile test, this transition zone in the

necking region became slightly opaque, indicating the formation of a heterogeneous

structure. Here, we examine the structure in this transition zone using the MET. The re-

swollen shape of the DN gel around this transition zone (after a stretch of ε = 6.93) is

illustrated in **Figure 7a**. **Figure 7b** shows the depth profile of the electric potential in

the transition zone measured from a non-cut surface. For comparison, the results for the

softened zone and unsoftened zone are also shown. In contrast to the electric potential

in the softened and unsoftened zones, the electric potential in the transition zone shows

a much thicker gradient layer (~ 75 μm), connecting the skin with the same electric

potential as the softened zone and the bulk with electric potential shown in **Table 2**.

T

h

e

926 that in the un-softened zone. This result implies that the damage initiates from the
927 surface, and then propagates through the depth of the gels. Moreover, the potential
928 fluctuation is also found to be more significant in this gradient layer than in the depth,
929 showing the fragmentation of the PAMPS networks.
930

931 ## Conclusions

932 We employ the MET to study the internal fracture behavior of the pre-stretched
933 DN gel under uniaxial deformation. This method gives structure information at a scale
934 larger than the probe size of ~200 nm in this study. The measured electric potential
935 distributions in re-swollen DN gels reveal the stretch-induced anisotropy: the material
936 is softened more significantly along the tensile direction, possibly related to the
937 coalescence of the internal cracks on the first network. With the increase of pre-stretch,
938 the statistical distribution of potential values changes from unimodal to bimodal,
939 indicating the coexistence of minor damaged parts and the major damaged parts. The
940 volume fraction, α, of the minor damaged part is predicted to decrease with the increase
941 of pre-stretch strain, while the volume fraction of the major damaged part increases
942 with stretch and reaching 0.72 in the hardening regime. The average distance between
943 neighboring major (or minor) damaged parts along the tensile direction are almost
944 constant at ~2 μm for the un-swollen sample, independent of the pre-stretch strain.
945 Additionally, the microstructure of the transition region between the necked and un-
946 necked zones suggests that the damage initiates from the gel surface and then
947 propagates into the depth.

ASSOCIATED CONTENT

The Supporting Information is available free of charge on the ACS Publications website at DOI: @@@.

The measured electric potential of virgin DN gel with microelectrodes of different tip diameters, **Figure S1**. Image of the pre-stretched DN gel under polarized optical observation by tensile test, **Figure S2**; Image of the transition zone under polarized optical microscope, **Figure S3**. (PDF)

AUTHOR INFORMATION

Corresponding Author: Jian Ping Gong, +81-11-706-9011, E-mail: gong@sci.hokudai.ac.jp

ACKNOWLEDGMENTS

This research was supported by JSPS KAKENHI Grant Numbers JP17H06144, 17H06376. Institute for Chemical Reaction Design and Discovery (ICReDD) was established by World Premier International Research Initiative (WPI), MEXT, Japan. The authors thank Dr. Feng Luo and Ms. Runa Kawakami for the helpful discussion on the DN fracture behavior, as well as Dr. Youfeng Yue, Dr. Abu Bin Ihsan, Dr. Saika Ahmed, Dr. Yiwan Huang, Mr. Nishimura and Ms. Liang Chen for their kind help with the experiments.

The authors declare no competing financial interest.

References

(1) Jen A. C.; Wake M. C.; Mikos A. G. Review: hydrogels for cell immobilization, *Bitechnology and Bioengineering*, **1996**, 50, 357-364 DOI: 10.1002/(sici)1097-0290(19960520)50:4<357::aid-bit2>3.0.co;2-k

(2) Gong, J. P.; Katsuyama, Y.; Kurokawa, T.; Osada, Y. Double-Network Hydrogels with Extremely High Mechanical Strength. *Adv. Mater.* **2003**, *15* (14), 1155–1158 DOI: 10.1002/adma.200304907.

(3) Yasuda, K.; Gong, J. P.; Katsuyama, Y.; Nakayama, A.; Tanabe, Y.; Kondo, E.; Ueno, M.; Osada, Y. Biomechanical Properties of High-Toughness Double Network Hydrogels. *Biomaterials* **2005**, *26* (21), 4468–4475 DOI: 10.1016/j.biomaterials.2004.11.021.

(4) Gong, J. P. Why Are Double Network Hydrogels so Tough? *Soft Matter* **2010**, *6* (12), 2583 DOI: 10.1039/b924290b.

(5) Nakajima, T.; Sato, H.; Zhao, Y.; Kawahara, S.; Kurokawa, T. A Universal Molecular Stent Method to Toughen Any Hydrogels Based on Double Network Concept. *Adv. Funct. Mater.* **2012**, *22*, 4426–4432 DOI: 10.1002/adfm.201200809.

(6) Ducrot, E.; Chen, Y.; Bulters, M.; Sijbesma, R. P.; Creton, C. Toughening Elastomers with Sacrificial Bonds and Watching Them Break. *Science (80-.).* **2014**, *344* (6180), 186–189 DOI: 10.1126/science.1248494.

(7) Ducrot, E.; Montes, H.; Creton, C. Structure of Tough Multiple Network Elastomers by Small Angle Neutron Scattering. *Macromolecules* **2015**, *48* (21), 7945–7952 DOI:

10.1021/acs.macromol.5b01979.

(8) Na, Y. H.; Tanaka, Y.; Kawauchi, Y.; Furukawa, H.; Sumiyoshi, T.; Gong, J. P.; Osada, Y. Necking Phenomenon of Double-Network Gels. *Macromolecules* **2006**, *39* (14), 4641–4645 DOI: 10.1021/ma060568d.

(9) Webber, R. E.; Creton, C.; Brown, H. R.; Gong, J. P. Large Strain Hysteresis and Mullins Effect of Tough Double-Network Hydrogels. *Macromolecules* **2007**, *40* (8), 2919–2927 DOI: 10.1021/ma062924y.

(10) Diani, J.; Fayolle, B.; Gilormini, P.; Diani, J.; Fayolle, B.; Gilormini, P.; Polymer, E. A Review on the Mullins Effect To Cite This Version : *Eur. Polym. J.* **2009**, 601–612.

(11) Mullins, L. Softening of Rubber by Deformation. *Rubber Chemistry and Technology*. 1969, pp 339–362.

(12) Nakajima, T.; Kurokawa, T.; Ahmed, S.; Wu, W.; Gong, J. P. Characterization of Internal Fracture Process of Double Network Hydrogels under Uniaxial Elongation. *Soft Matter* **2013**, *9* (6), 1955–1966 DOI: 10.1039/C2SM27232F.

(13) Na, Y. H.; Kurokawa, T.; Katsuyama, Y.; Tsukeshiba, H.; Gong, J. P.; Osada, Y.; Okabe, S.; Karino, T.; Shibayama, M. Structural Characteristics of Double Network Gels with Extremely High Mechanical Strength. *Macromolecules* **2004**, *37* (14), 5370–5374 DOI: 10.1021/ma049506i.

(14) Tsukeshiba, H.; Huang, M.; Na, Y. H.; Kurokawa, T.; Kuwabara, R.; Tanaka, Y.; Furukawa, H.; Osada, Y.; Gong, J. P. Effect of Polymer Entanglement on the Toughening of Double Network Hydrogels. *J. Phys. Chem. B* **2005**, *109* (34), 16304–16309 DOI: 10.1021/jp052419n.

(15) Nakajima, T.; Furukawa, H.; Tanaka, Y.; Kurokawa, T.; Gong, J. P. Effect of Void Structure on the Toughness of Double Network Hydrogels. *J. Polym. Sci. Part B Polym. Phys.* **2011**, *49* (17), 1246–1254 DOI: 10.1002/polb.22293.

(16) Nakajima, T.; Furukawa, H.; Gong, J. P.; Lin, E. K.; Wu, W. L. A Deformation Mechanism for Double-Network Hydrogels with Enhanced Toughness. *Macromol. Symp.* **2010**, *291–292* (1), 122–126 DOI: 10.1002/masy.201050515.

(17) Tominaga, T.; Tirumala, V. R.; Lin, E. K.; Gong, J. P.; Furukawa, H.; Osada, Y.; Wu, W. li. The Molecular Origin of Enhanced Toughness in Double-Network Hydrogels: A Neutron Scattering Study. *Polymer (Guildf).* **2007**, *48* (26), 7449–7454 DOI: 10.1016/j.polymer.2007.10.016.

(18) Liang, S.; Hu, J.; Wu, Z. L.; Kurokawa, T.; Gong, J. P. Toughness Enhancement and Stick-Slip Tearing of Double-Network Hydrogels in Poly(Ethylene Glycol) Solution. *Macromolecules* **2012**, *45* (11), 4758–4763 DOI: 10.1021/ma300357f.

(19) Takahata, T.; Hayashi, M.; Ishikawa, T. SK4/IK1-like Channels Mediate TEA-Insensitive, Ca2+-Activated K+ Currents in Bovine Parotid Acinar Cells. *Am. J. Physiol. Cell Physiol.* **2003**, *284* (1), C127-44 DOI: 10.1152/ajpcell.00250.2002.

(20) Guo, H.; Kurokawa, T.; Takahata, M.; Hong, W.; Katsuyama, Y.; Luo, F.; Ahmed, J.; Nakajima, T.; Nonoyama, T.; Gong, J. P. Quantitative Observation of Electric Potential Distribution of Brittle Polyelectrolyte Hydrogels Using Microelectrode Technique. *Macromolecules* **2016**, *49* (8), 3100–3108 DOI: 10.1021/acs.macromol.6b00037.

(21) Nakajima, T.; Furukawa, H.; Tanaka, Y.; Kurokawa, T.; Osada, Y.; Gong, J. P. True

Chemical Structure of Double Network Hydrogels. *Macromolecules* **2009**, *42* (6), 2184–2189 DOI: 10.1021/ma802148p.

(22) Donnan, F. G. Theorie Der Membrangleichgewichte Und Membranpotentiale Bei Vorhandensein von Nicht Dialysierenden Elektrolyten. Ein Beitrag Zur Physikalisch-chemischen Physiologie (The Theory of Membrane Equilibrium and Membrane Potential in the Presence of a Non-Dialyz. *Zeitschrift Elektrochem. Angew. Phys.Chem.* **1911**, *17* (14), 572–581 DOI: 10.1002/bbpc.19110171405.

(23) Tominaga, T.; Tirumala, V. R.; Lee, S.; Lin, E. K.; Gong, J. P.; Wu, W. L. Thermodynamic Interactions in Double-Network Hydrogels. *J. Phys. Chem. B* **2008**, *112* (13), 3903–3909 DOI: 10.1021/jp710284e.

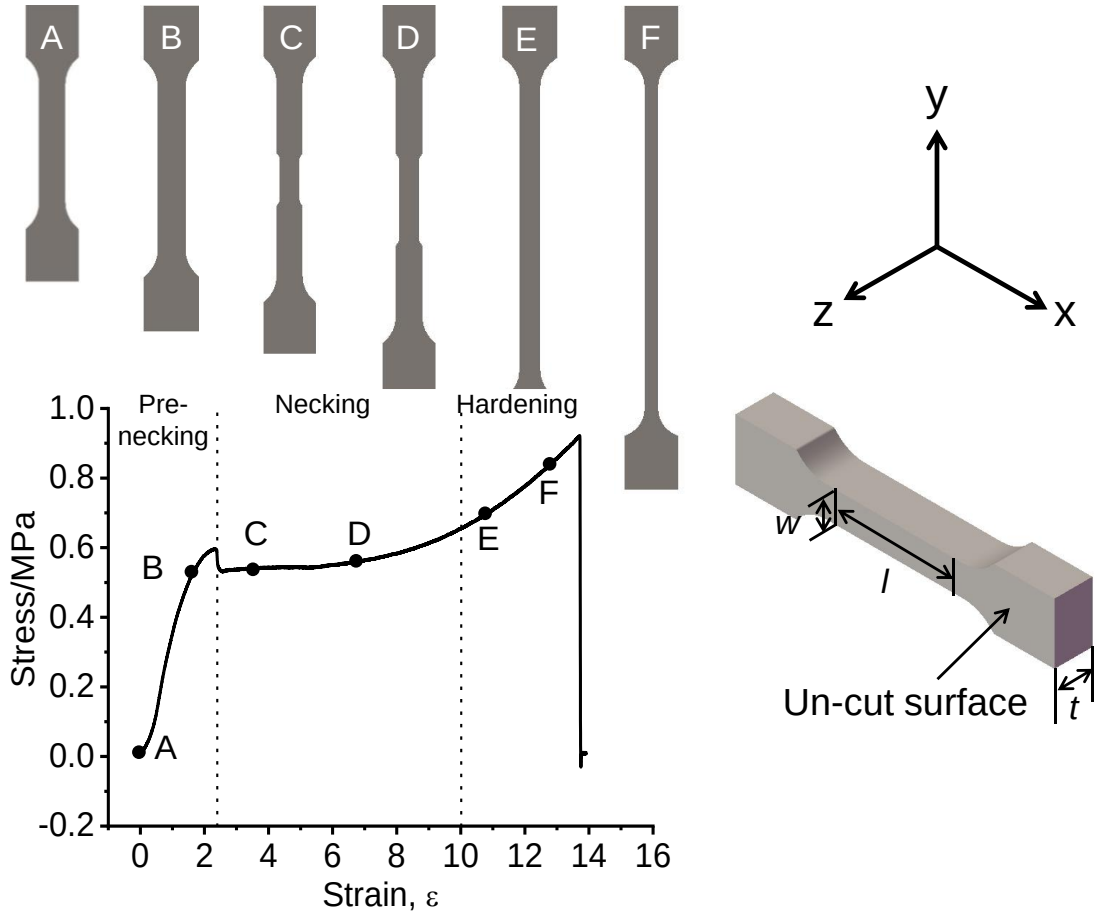

Figure 1. Loading curve of a typical DN gel under uniaxial elongation. The curve has three characteristic regimes of deformation: pre-necking, necking, and hardening, as shown by the vertical dotted lines. The schematic illustrations above the loading curve show the shapes of the sample in these three regimes. The right figure shows the 3D illustration of the dumbbell shape sample and the coordinates used in this study. The *w*, *l* and *t* represent the width, length and thickness of the DN sample, respectively. The tensile direction is defined as parallel to the x-axis, the width direction and the thickness direction of the sample are defined as parallel to y-axis and z-axis, respectively. The sample surface in x,y-plane is the un-cut surface, and those in y,z- and x,z-planes are cut surfaces. The tensile test was performed at 100 mm/min.

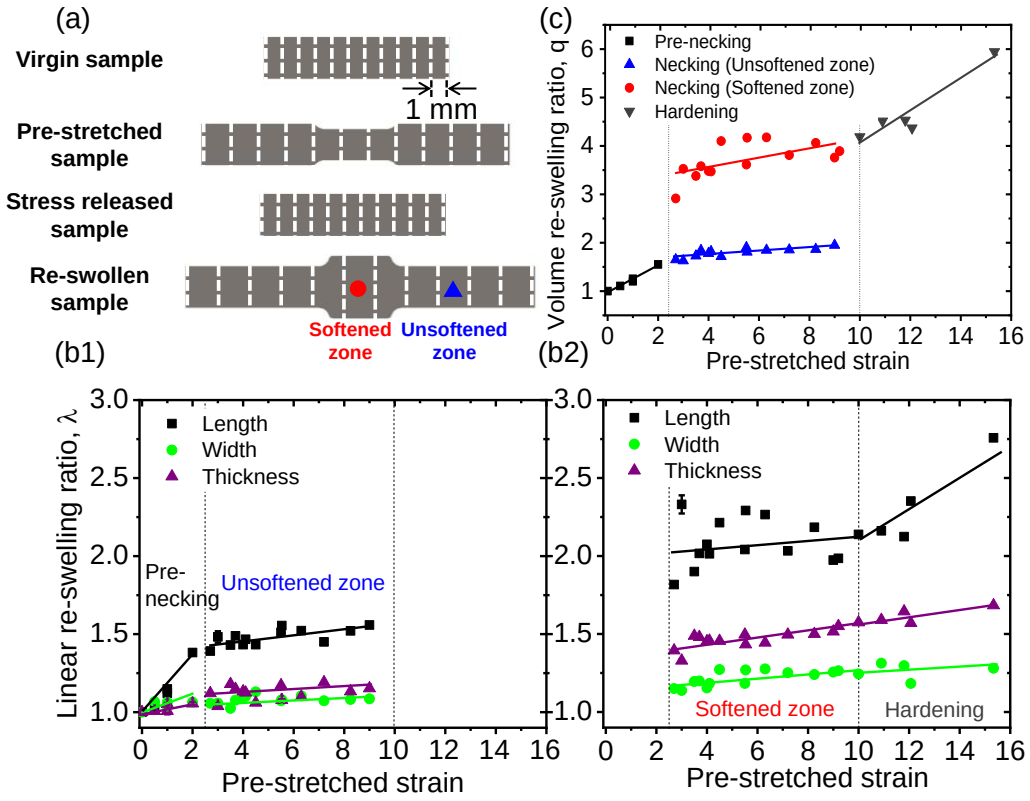

Figure 2. (a) Schematic illustrations showing the shape change of the sample. The red dot and blue triangle represent the softened (necked) zone and the unsoftened (un-necked) zone, respectively in the necking regime. The vertical white dash lines indicate the markers with 1 mm intervals used to measure the local re-swelling ratios at various positions. (b) Linear re-swelling ratios λ in length, width, and thickness of the pre-stretched DN gel at pre-necking regime and unsoftened zones of necking regime (b1), and at softened zone of necking regime and hardening regime (b2). (c) Volume re-swelling ratio q by volume of the samples after being pre-stretched at different maximum strains. Owing to the internal fracture of the first polyelectrolyte network, the pre-stretched sample, especially in the softened zone, re-swells remarkably in water.

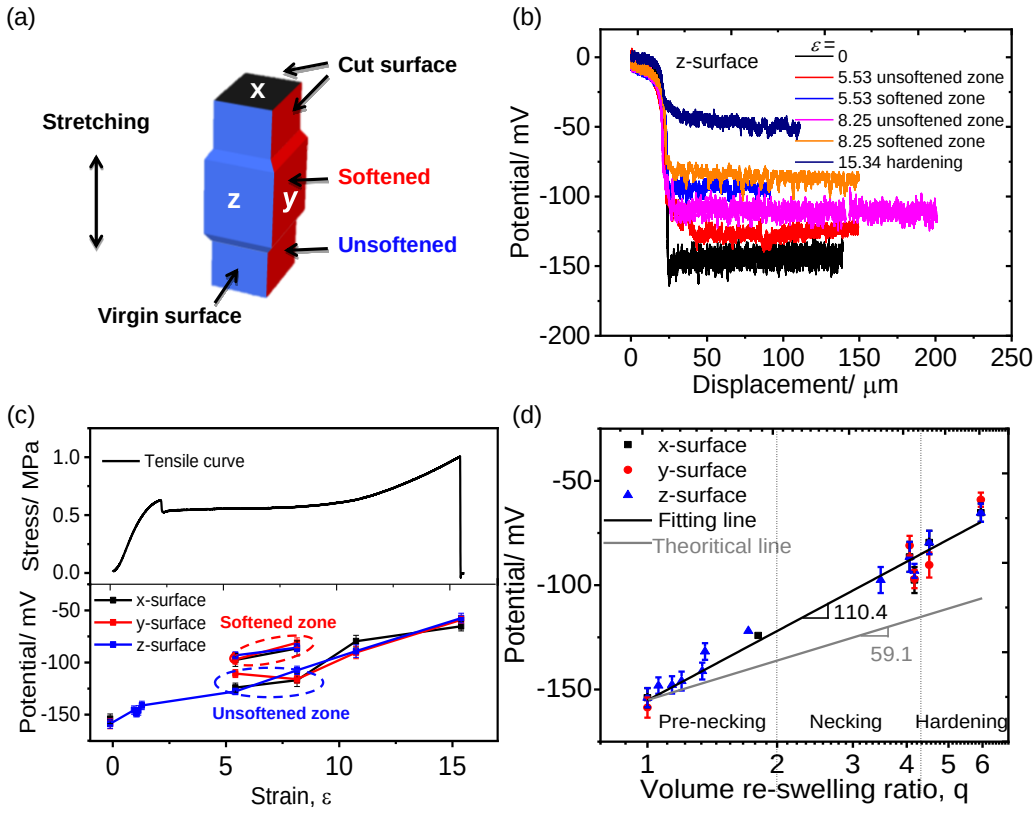

Figure 3. (a) Schematic illustration of three different surfaces of a pre-stretched DN gel used to measure the electric potential. For a necking sample, the softening and the unsoftened zone co-exist, and the softened zone underwent a larger swelling than the unsoftened zone in the reference solution. (b) Depth profiles of the electric potential measured by the microelectrode technique from the un-cut surface (x,y-plane) into the bulk of the DN hydrogel after unloaded from different strains ε. (c) Tensile stress and strain curve (top) and average bulk potentials of re-swelled samples pre-stretched at different strains detected from the three different surfaces (bottom). In the necking regime, the measurements were performed on both the softened zone and the unsoftened zone. (d) Correlation between the bulk re-swelling ratio q and the electric potential for pre-stretched DN gels re-swelled in the reference solution. The electric

potentials in necking regime were measured at the softened zone. The fitting line in the semi-log plot has a slope of 110 mV. The grey straight line is the theoretical curve from **Eq.2**. The effective salt concentration of reference solution was 4.4×10^{-5} M.

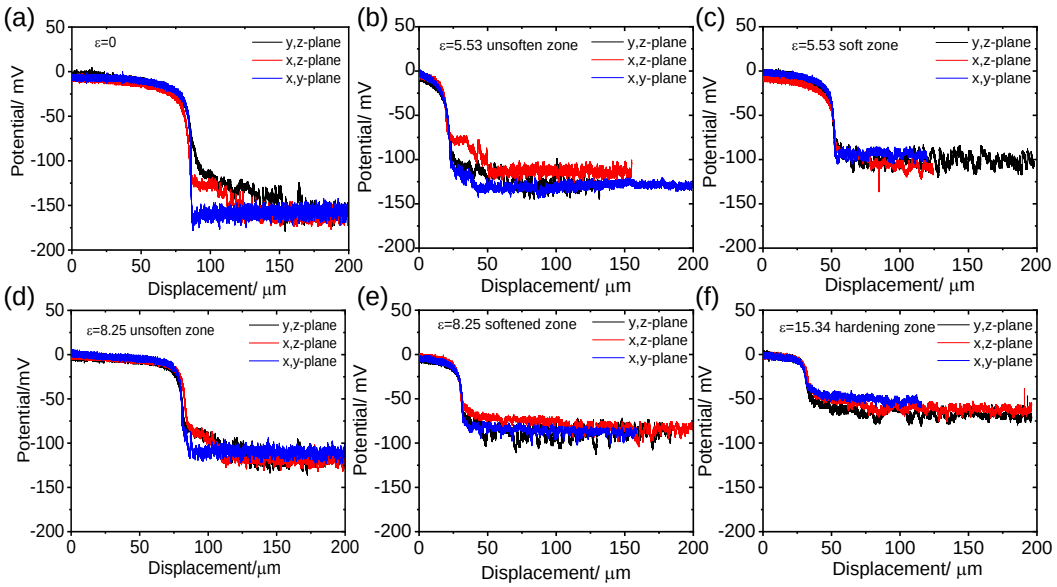

Figure 4. Depth profiles of the electrical potential measured from the y,z-, x,z- and x,y-planes of re-swelled DN gels at different pre-stretched regimes: (a) virgin sample (ε = 0); (b, c) necking regime (ε = 5.53), unsoftened zone (c) and softened zone (d); (d, e) necking regime (ε = 8.25), unsoftened zone (d) and softened zone (e); and (f) hardening regime (ε = 15.34). The y,z-, x,z- and x,y-planes are defined in **Figure 1**.

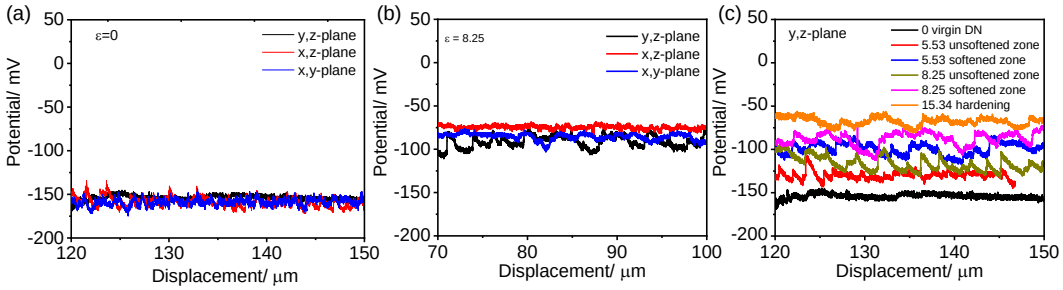

Figure 5. Potential fluctuation profiles for bulk DN gels, measured from the y,z-, x,z- and x,y-planes for (a) virgin samples and (b) in the softened zone of a sample pre-stretched to necking regime (ε = 8.25), as well as (c) from the y,z-plane at different pre-stretch strains. The horizontal axis is shifted for some data to allow comparison in the same observation window.

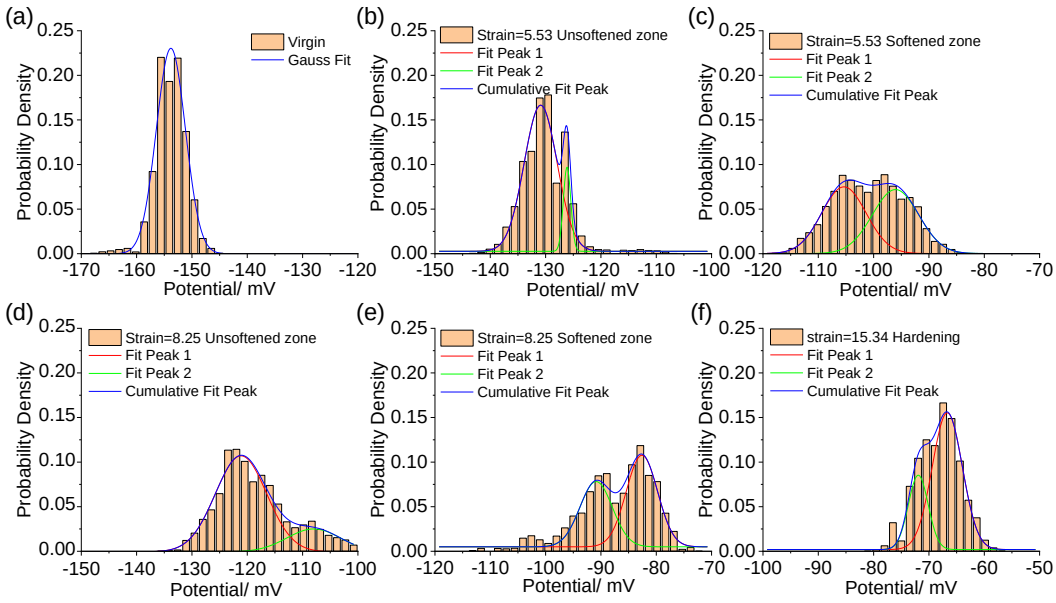

Figure 6. Statistical analysis of the electrical potential values measured from the y,z-plane of DN gel subjected to different pre-stretch strains. The probability densities are fitted to unimodal or bimodal Gaussian distributions. The sampling step for the histograms is 1.5 mV. The statistical data are summarized from the raw data shown in **Figure 5c**.

Table 1. Peak positions, FWHM (*w*), and integral area fraction of peak 1, α, obtained from **Figure 6** with the Gaussian function at different pre-stretched strains. $f_A = A_1/(A_1 + A_2)$, where A_1 and A_2 are the integral area of high potential peak (peak 1) and low potential peak (peak 2), respectively.

Sample	virgin	necking				hardening
	ε=0	ε=5.53 unsoftened zone	ε=5.53 softened zone	ε=8.25 unsoftened zone	ε=8.25 softened zone	ε=15.34
Peak 1/ mV	-153.8	-130.9	-105.4	-121.1	-90.9	-71.9
Peak 2/ mV	-	-126.1	-96.0	-108.0	-82.6	-66.7
w_1/ mV	5.26	5.94	8.04	9.27	5.88	3.58
w_2/ mV	-	1.35	8.37	9.67	5.65	5.44
f_A	1.00	0.88	0.50	0.80	0.42	0.26

Table 2. Structure parameters calculated from potential data using a simplified bimodal model.

Strain	necking				hardening
	5.53 (unsoftened)	5.53 (softened)	8.25 (unsoftened)	8.25 (softened)	15.53
q_1 (cal.)	1.61	2.75	1.98	3.85	5.73
q_2 (cal.)	1.78	3.35	2.61	4.52	6.32
q (cal.)	1.63	3.02	2.08	4.21	6.16
q (exp.)[1)]	1.80	3.88	1.86	4.06	5.94
α (cal.)	0.88	0.50	0.80	0.42	0.26
α_0 (cal.)	0.89	0.55	0.84	0.46	0.28
ξ (exp.) (μm)[2)]	-	4.46 ±2.52	-	4.66 ±3.26	5.66 ±4.45
ξ_0 (cal.) (μm)[3)]	-	1.95	-	2.14	2.06

[1)]: Measured from bulk size change of the DN gels; [2)]: The potential fluctuation length in stretch direction; [3)]: $\xi_0 = \xi/\lambda_l$ where λ_l is the linear re-swelling ratio in the stretching direction.

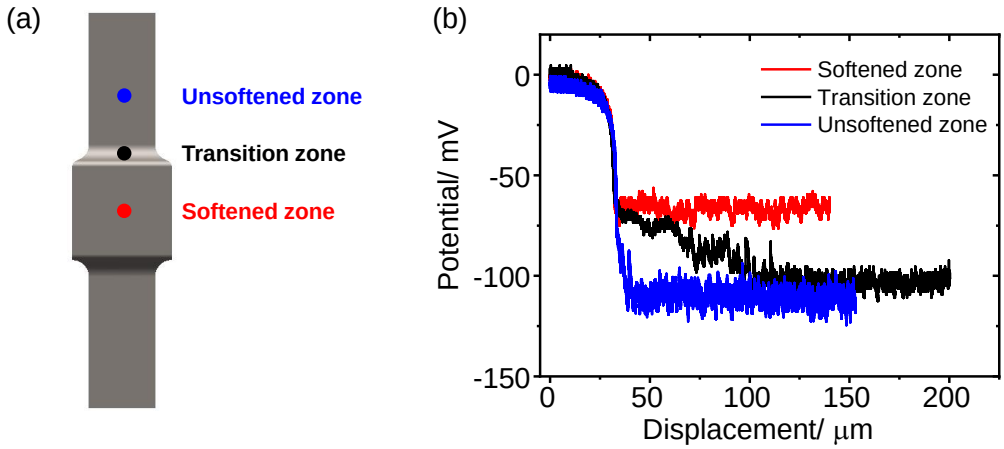

Figure 7. (a) Schematic illustration of a necked sample in the re-swollen state. After re-swelling, the unsoftened zone, transition zone, and softened zone of the sample could be distinguished according to the swelling degree. The dots show the positions where the potentials were measured. (b) Electric potential profiles measured from the non-cut surface of the sample, in the softened zone, transition zone and unsoftened zone. The potential profile of the transition zone suggests that the internal damage initiates from the surface to the depth.

Supporting information

Internal Damage Evolution in Double-Network Hydrogels Studied by Microelectrode Technique

Honglei Guo[1,2], Wei Hong[3,2,4], Takayuki Kurokawa[1,2], Takahiro Matsuda[5], Zi Liang Wu[1,6], Tasuku Nakajima[1,2,7], Masakazu Takahata[8], Taolin Sun[1,2,9], Ping Rao[5], Jian Ping Gong[1,2,7]*

[1]Faculty of Advanced Life Science, Hokkaido University, Sapporo, 001-0021, Japan

[2]Soft Matter GI-CoRE, Hokkaido University, Sapporo, Japan

[3]Department of Mechanics and Aerospace Engineering, Southern University of Science and Technology, Shenzhen, 518055, China

[4]Department of Aerospace Engineering, Iowa State University, Ames, Iowa 50011, United States

[5]Graduate School of Life Science, Hokkaido University, Sapporo, 001-0021, Japan

[6]Ministry of Education Key Laboratory of Macromolecular Synthesis and Functionalization, Department of Polymer Science and Engineering, Zhejiang University, Hangzhou 310027, China

[7]Institute for Chemical Reaction Design and Discovery (WPI-ICReDD), Hokkaido University, N21W10, Kita-ku, Sapporo, Hokkaido, 001-0021, Japan

[8]Faculty of Science, Hokkaido University, Sapporo, 060-0810, Japan

[9]South China Advanced Institute for Soft Matter Science and Technology, South China University of Technology, Guangzhou 510640, China

*Corresponding author

Telephone/Fax: +81-11-706-9011, E-mail: gong@sci.hokudai.ac.jp

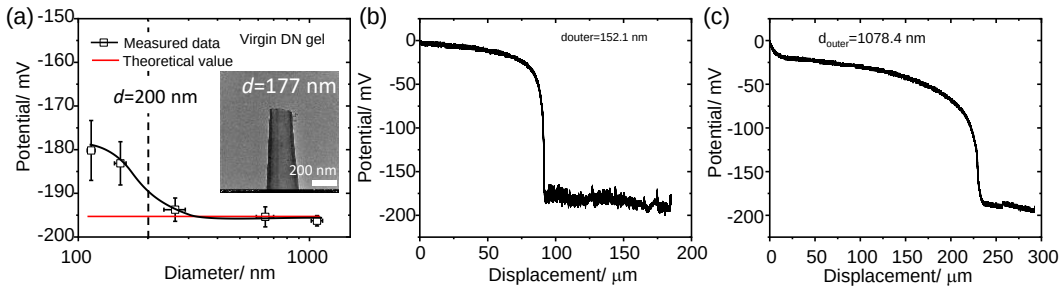

Figure S1. (a) The measured electric potential of the virgin DN gel by using microelectrodes of different tip diameters. The horizontal red line indicates the theoretical potential estimated from **Eq. (1)** by using the bulk concentration of PAMPS in the virgin DN gel (C_g = 1/19.7 M), the KCl concentration (C_s =10^{-5} M), the activity coefficient (γ_g = 0.35, γ_s = 1.0). A typical TEM image of the glass capillary (d_{outer} =177 nm) is shown in it. (b) The measured potential curve of the virgin DN gel by using a thin microelectrode (d_{outer}=152.1 nm). (c) The measured potential curve of the virgin DN gel by using a thick microelectrode (d_{outer}=1078.4 nm). In this experiment, the residual chemicals are carefully removed to a level less than 10^{-5} M by washing the samples in deionized water for more than one month before the potential measurement.

In situ optical observation of necking process

To observe the change in the orientation degree of the network strands during necking, two pieces of circular polarized films were fixed on the front of a video and a white lamp.[S1] The video camera recorded the shape and isochromatic images of the samples during test. The optical retardation change of the samples during the tensile test was estimated by comparing the birefringence colors using a Michel-Levy chart.[S2]

This simple method roughly indicated the stress distribution of the samples during deformation but provided no information regarding the stress direction.

Circular polarized optical observation in necking region

To understand why the re-swelling ratio in the softened zone increases with the pre-stretching strain, we observed the optical polarization of the sample during a tensile test with a pair of circular polarizing films. Under the circularly polarized light, the birefringence of the anisotropic DN gel can be estimated during stretching. **Figure S2** shows the polarized optical images of the DN gel at various strains. With the increase of the stretching, the retardation in the necked zone, as shown by the blue arrows, increases, reflecting the increase of the stress concentration. Furthermore, the retardation in the necked zone is not homogeneous, even at a high strain ($\varepsilon = 8.33$). Because the retardation is directly proportional to the true stress, the results indicate that the true stress applied in the necked zone varies with respect to the strain. That is, the increase of the true stress in the necked zone further breaks the PAMPS fragments into smaller sizes, increasing the re-swelling ratio in the softened zone. This result further explains the previous result that the initial elastic moduli of pre-stretched DN gels slightly decreases at a large pre-strain in necking stage.[12]

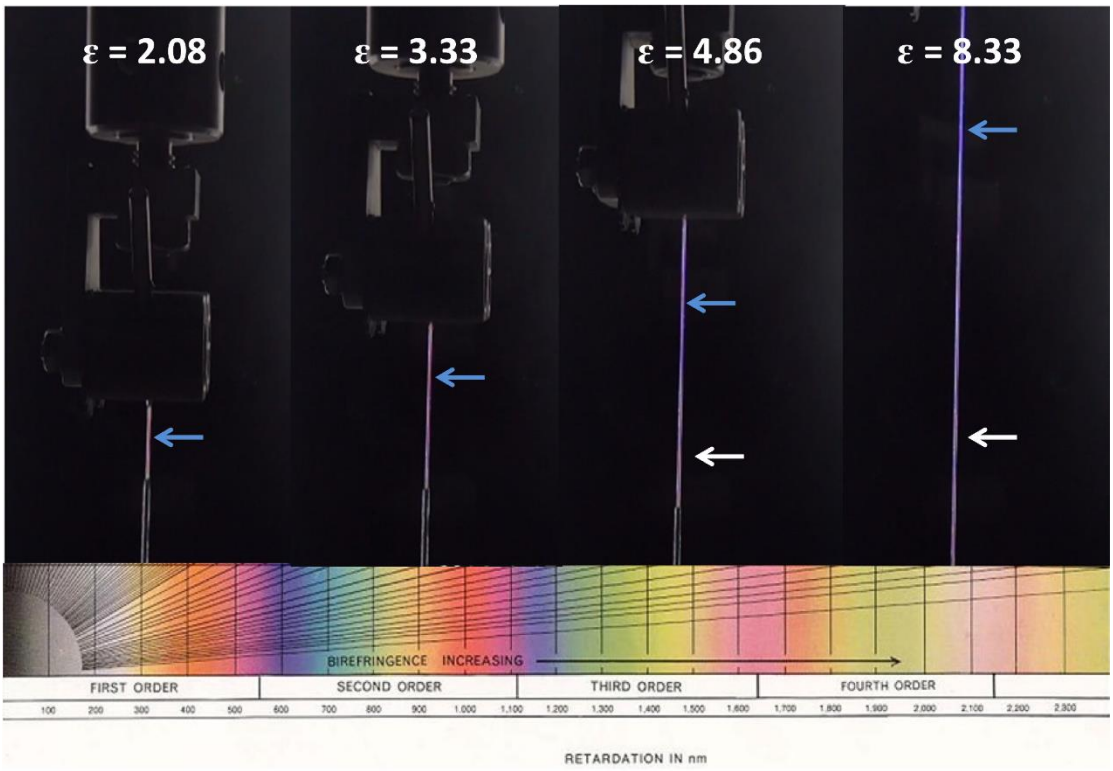

Figure S2. Birefringence images of the DN gel during the uniaxial elongation. The necking zone propagates with the increase of the strain. The birefringence color in the necking zone slightly changes with respect to the strain (blue arrows) and varies with respect to the position (white arrows), indicating that the orientation degree increases with the increase of the stretching and that the stretching is not homogeneous even in the necking region. The images were obtained via *in situ* observed by circular polarized optical observation during the uniaxial elongation.

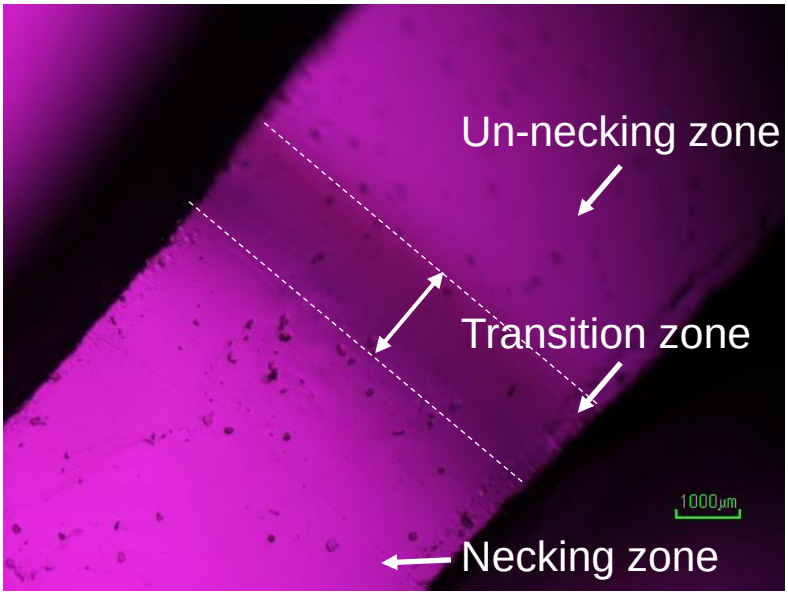

Figure S3. Image of the pre-stretched DN gel at ε = 3.8, obtained using a linear polarized optical microscope. A weakly ordered structure is observed in the transition zone. The observation was performed in the relaxed state of the sample without re-swelling.

References

(S1) Luo, F.; Sun, T. L.; Nakajima, T.; Kurokawa, T.; Zhao, Y.; Ihsan, A. Bin; Guo, H. L.; Li, X. F.; Gong, J. P. Crack Blunting and Advancing Behaviors of Tough and Self-Healing Polyampholyte Hydrogel. *Macromolecules* **2014**, *47*, 6037–6046.

(S2) Robert Hoffman and Michael W. Davidson, Michel-Levy Birefringence Chart. https://www.olympus-lifescience.com/en/microscope-resource/primer/techniques/polarized/michel/.